J. Fluid Mech. (2006), *vol.* 565, *pp.* 441–459. © 2006 Cambridge University Press
doi:10.1017/S0022112006001868 Printed in the United Kingdom

Shallow cavity flow in a porous medium driven by differential heating

By P. G. DANIELS

Centre for Mathematical Science, City University, Northampton Square, London EC1V 0HB, UK

(Received 13 October 2005 and in revised form 24 April 2006)

This paper describes steady flow through a porous medium in a shallow two-dimensional cavity driven by differential heating of the upper surface. The lower surface and sidewalls of the cavity are thermally insulated. The main emphasis is on the situation where the Darcy–Rayleigh number R is large and the aspect ratio of the cavity L (length/depth) is of order $R^{1/2}$. For a monotonic temperature distribution at the upper surface, the leading-order problem consists of an interaction involving the horizontal boundary-layer equations, which govern the flow throughout most of the cavity, and the vertical boundary-layer equations which govern the flow near the colder sidewall. This problem is solved using numerical and asymptotic methods. The limiting cases where $L \gg R^{1/2}$ and $L \ll R^{1/2}$ are also discussed.

1. Introduction

In many thermally driven porous media flows such as those encountered in geothermal energy systems the lateral extent d of the solid/fluid layer is much greater than the depth h. For such layers heated uniformly from below the instability of the flow at finite values of the Darcy–Rayleigh number R (defined in (2.3) below) is of major interest and the extensive body of work in this area stemming from the original analysis of Lapwood (1948) has been reviewed recently by Rees (2000). For two-dimensional cavities differentially heated at the sides, Walker & Homsy (1978) obtained steady solutions for the shallow cavity limit where the aspect ratio $L = d/h \to \infty$ with R finite. Daniels, Blythe & Simpkins (1986, 1989) considered the case where the upper and lower surfaces are thermally insulated and the Darcy–Rayleigh number is large. They identified two main asymptotic regimes, the so-called merged-layer regime where $L = O(R^{1/2})$ and the intermediate regime where $L = O(R)$. The merged-layer limit is characterized by the fact that the double horizontal layers which exist near the insulated surfaces when $L = O(1)$ and $R \gg 1$ merge to fill the cavity. In practice, the merged-layer regime is important because it covers the vast majority of the R, L parameter space as $R \to \infty$ (Blythe, Simpkins & Daniels 1983).

In many geothermal applications it is not appropriate to consider the horizontal surfaces to be thermally insulated. The present paper is concerned with developing an understanding of the high Darcy–Rayleigh number structure of steady shallow cavity flows driven by differential heating at the horizontal surfaces. The simplest situation to consider is where only the upper surface is heated, with the other three acting passively as thermal insulators. Progress with this problem has been made by Daniels & Punpocha (2004) who reported numerical solutions for Darcy–Rayleigh numbers in the range $0 < R \leqslant 5000$ and aspect ratios $\frac{1}{4} \leqslant L \leqslant 4$. These results indicated that

https://doi.org/10.1017/S0022112006001868 Published online by Cambridge University Press

for monotonic differential heating a single-cell circulation is generated, the centre of which moves towards the upper cold corner of the cavity as R increases. The asymptotic structure of the flow for finite L and large R has been described by Daniels & Punpocha (2005). In this limit the main circulation is completed within a horizontal boundary layer of depth $O(R^{-1/3}L^{2/3}h)$ near the upper surface and a vertical boundary layer of width $O(R^{-2/3}L^{1/3}h)$ near the cold sidewall. Fluid from the horizontal layer is entrained by the vertical boundary layer where it descends and is detrained back to the horizontal layer. A weaker circulation is also generated in the core region below, which to leading order is at a constant temperature somewhat higher than the minimum temperature of the upper surface. The core temperature is determined by the (interactive) solution of the two boundary-layer problems.

The theory of Daniels & Punpocha (2005) breaks down in the limit $L \to \infty$ because the horizontal-layer depth becomes comparable with the depth of the cavity when $L = O(R^{1/2})$. In the present paper this regime is investigated and the main properties of the solution are determined. The problem is formulated in § 2 and the main features of the asymptotic structure as $R \to \infty$ are outlined in § 3. This structure consists of a core region governed by the horizontal boundary-layer equations and a vertical boundary layer near the colder sidewall. Asymptotic properties of the solution near the upper and lower surfaces of the cavity are discussed in § 4 and assist in the construction of a suitable numerical scheme for solving the interactive boundary-layer problem, which is described in § 5. The results are given in § 6, and § 7 includes a discussion of the limiting cases $LR^{-1/2} \to 0$ and $LR^{-1/2} \to \infty$.

2. Formulation

A rectangular two-dimensional cavity $0 \leqslant x^* \leqslant d, 0 \leqslant z^* \leqslant h$ is filled with a fluid-saturated porous medium. The upper boundary $z^* = h$ is held at temperature

$$T^* = T_0^* + \Delta T S(x^*/d), \tag{2.1}$$

where the function $S(x^*/d)$ varies monotonically from zero at $x^* = 0$ to 1 at $x^* = d$. The vertical walls $x^* = 0$ and $x^* = d$ and the bottom wall $z^* = 0$ are thermally insulated. Subject to Darcy's law and the Oberbeck–Boussinesq approximation, steady two-dimensional motion is governed by the non-dimensional equations

$$\nabla^2 \psi = -R \frac{\partial T}{\partial x}, \quad \nabla^2 T = \frac{\partial(T, \psi)}{\partial(x, z)}, \tag{2.2}$$

where $\nabla^2 = \partial^2/\partial x^2 + \partial^2/\partial z^2$, $\psi(x, z)$ is the stream function non-dimensionalized by the thermal diffusivity κ, $T(x, z)$ is the temperature measured relative to T_0^* and non-dimensionalized by ΔT, (x, z) are Cartesian coordinates non-dimensionalized by h, and R is the Darcy–Rayleigh number defined by

$$R = Kg\bar{\beta}\Delta T h/\kappa\nu, \tag{2.3}$$

where K is the permeability, $\bar{\beta}$ is the coefficient of thermal expansion, ν is the kinematic viscosity and g is the acceleration due to gravity. The non-dimensional velocity components in the x-, z-directions are given by

$$u = \frac{\partial \psi}{\partial z}, \quad w = -\frac{\partial \psi}{\partial x} \tag{2.4}$$

respectively.

https://doi.org/10.1017/S0022112006001868 Published online by Cambridge University Press

The cavity walls are assumed to be impermeable, so that the boundary conditions are

$$\psi = \frac{\partial T}{\partial x} = 0 \text{ on } x = 0, L, \tag{2.5}$$

$$\psi = \frac{\partial T}{\partial z} = 0 \text{ on } z = 0, \tag{2.6}$$

$$\psi = 0, \quad T = S(x/L) \text{ on } z = 1. \tag{2.7}$$

Solutions of the problem defined by (2.2) and (2.5)–(2.7) depend on the Darcy–Rayleigh number R and the aspect ratio $L = d/h$, and also on the specific form of the temperature profile $S(x/L)$ at the upper surface, which is taken to be

$$S(x/L) = 1 - \left(1 - \frac{x}{L}\right)^2. \tag{2.8}$$

Note that because the bottom wall and sidewalls of the cavity are thermally insulated, the total heat flux through the upper surface is zero:

$$\int_0^L \frac{\partial T}{\partial z}(x, 1)\,\mathrm{d}x = 0. \tag{2.9}$$

Numerical solutions of the above problem have been reported by Daniels & Punpocha (2004) and the asymptotic structure of the solution as $R \to \infty$ has been described by Daniels & Punpocha (2005). The monotonic temperature profile (2.8) is chosen to coincide with that used in these earlier papers; other monotonic forms are not expected to result in any qualitative changes to the solution.

The present paper is concerned with the limiting form of the solution of (2.2) and (2.5)–(2.7) as $R \to \infty$ for aspect ratios L such that the parameter

$$\bar{L} = LR^{-1/2} \tag{2.10}$$

is finite. The main reason for assuming a monotonic profile (2.8) is that at large Darcy–Rayleigh numbers the flow descends in a boundary layer adjacent to the colder wall. For non-monotonic temperature profiles this boundary layer is expected to detach from the cold wall to form a free shear layer below the position of minimum temperature. Indeed, the solutions to be obtained here can be viewed in just this way if the profile (2.8) is extended as an even function in $-L \leqslant x \leqslant 0$. This is because the conditions (2.5) at $x = 0$ are then equivalent to symmetry conditions on the centreline of the extended domain $-L \leqslant x \leqslant L$. Solutions for the free shear layer problem in the case of an asymmetric, non-monotonic temperature profile are not considered here.

3. Asymptotic solution as $R \to \infty$

The main features of the asymptotic structure of the solution as $R \to \infty$ are shown schematically in figure 1. In the core region $0 < x \leqslant L, 0 \leqslant z \leqslant 1$,

$$T(x, z) = \bar{\theta}(X, z) + \cdots, \quad \psi(x, z) = R^{1/2}\bar{\phi}(X, z) + \cdots, \tag{3.1}$$

where $x = R^{1/2}X$ and $\bar{\theta}$ and $\bar{\phi}$ satisfy the horizontal boundary-layer equations

$$\frac{\partial^2 \bar{\phi}}{\partial z^2} = -\frac{\partial \bar{\theta}}{\partial X}, \quad \frac{\partial^2 \bar{\theta}}{\partial z^2} = \frac{\partial \bar{\phi}}{\partial z}\frac{\partial \bar{\theta}}{\partial X} - \frac{\partial \bar{\phi}}{\partial X}\frac{\partial \bar{\theta}}{\partial z}, \tag{3.2}$$

https://doi.org/10.1017/S0022112006001868 Published online by Cambridge University Press

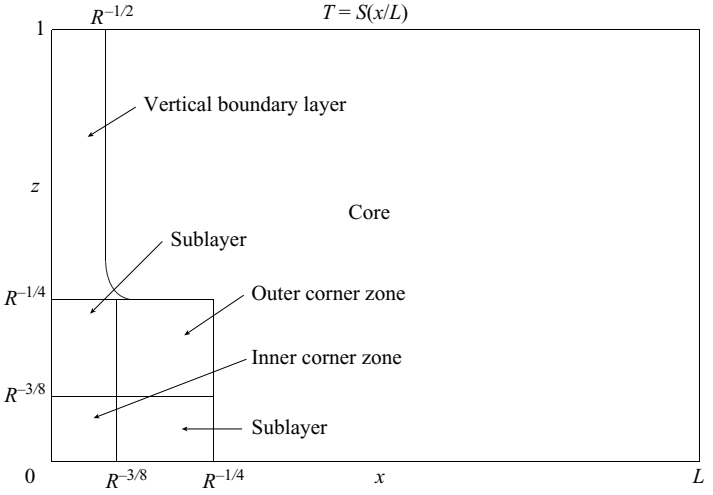


FIGURE 1. Schematic diagram showing the main regions of the asymptotic structure of the solution as $R \to \infty$.

with boundary conditions

$$\bar{\phi} = 0, \quad \bar{\theta} = 1 - \left(1 - \frac{X}{\bar{L}}\right)^2 \text{ on } z = 1, \tag{3.3}$$

$$\bar{\phi} = 0, \quad \frac{\partial \bar{\theta}}{\partial z} = 0 \text{ on } z = 0, \tag{3.4}$$

$$\bar{\phi} = \frac{\partial \bar{\theta}}{\partial X} = 0 \text{ on } X = \bar{L}. \tag{3.5}$$

Here (3.3) and (3.4) are the conditions at the upper and lower surfaces respectively, whilst (3.5) assumes that the two boundary conditions at the hotter sidewall apply directly to the horizontal boundary-layer solution, despite the fact that the highest derivatives in x do not appear in (3.2). This is partly because satisfaction of $\bar{\phi} = 0$ at $X = \bar{L}$ also guarantees satisfaction of $\partial\bar{\theta}/\partial X = 0$ at $X = \bar{L}$, from the first of equations (3.2). For the temperature profile in (3.3) the solution is regular at $X = \bar{L}, z = 1$, an advantage when solving the system numerically; profiles $S(x/L)$ for which the gradient is non-zero at $x = L$ would lead to a singular solution structure with $1 - z \sim (\bar{L} - X)^{1/2}$ as $X \to \bar{L}$.

At the colder sidewall there is a vertical boundary layer in which

$$T(x, z) = \theta(\xi, z) + \cdots, \quad \psi(x, z) = R^{1/2}\phi(\xi, z) + \cdots, \tag{3.6}$$

where $x = R^{-1/2}\xi$ and ϕ and θ satisfy the equations

$$\frac{\partial^2 \phi}{\partial \xi^2} = -\frac{\partial \theta}{\partial \xi}, \quad \frac{\partial^2 \theta}{\partial \xi^2} = \frac{\partial \phi}{\partial z}\frac{\partial \theta}{\partial \xi} - \frac{\partial \phi}{\partial \xi}\frac{\partial \theta}{\partial z}, \tag{3.7}$$

with boundary conditions

$$\phi = \theta = 0 \text{ on } z = 1, \tag{3.8}$$

$$\phi = \frac{\partial \theta}{\partial \xi} = 0 \text{ on } \xi = 0, \tag{3.9}$$

$$\phi \to \phi_\infty(z), \quad \theta \to \theta_\infty(z) \text{ as } \xi \to \infty. \tag{3.10}$$

https://doi.org/10.1017/S0022112006001868 Published online by Cambridge University Press

Here the condition (3.8) on θ at the upper surface follows because the function $S(x/L)$ is of order R^{-1} on the small lateral scale of the vertical boundary layer, whilst (3.9) are the boundary conditions on the sidewall. The profiles ϕ_∞ and θ_∞ at the edge of the vertical layer are to be determined as part of the solution and must match with the solution in the core, requiring that

$$\phi_\infty(z) = \bar{\phi}(0, z), \quad \theta_\infty(z) = \bar{\theta}(0, z). \tag{3.11}$$

The horizontal and vertical boundary-layer systems interact through the matching conditions (3.11) and cannot be solved independently. In § 4 below, solutions of the combined system are sought near the upper surface ($z \to 1$) and lower surface ($z \to 0$), and then in §§ 5 and 6 a full numerical solution is described.

It should be noted that in general the vertical boundary-layer equations (3.7) possess solutions with exponential decay to (3.10) of the form $\exp(-\lambda(z)\xi)$ where λ is a root of the quadratic equation $\lambda^2 + \lambda\phi'_\infty - \theta'_\infty = 0$ with positive real part. The roots are given by

$$\lambda = \lambda_\pm = \tfrac{1}{2}\left(-\phi'_\infty \pm (\phi'^2_\infty + 4\theta'_\infty)^{1/2}\right). \tag{3.12}$$

Assuming that $\phi_\infty(0) = \phi_\infty(1) = 0$ there will be a point z_1 such that $0 < z_1 < 1$ and $\phi'_\infty(z_1) = 0$. Thus, in order for (3.12) to provide at least one root with positive real part at $z = z_1$, it is necessary that $\theta'_\infty(z_1) > 0$. Physically speaking, this ensures that the temperature field is stably stratified where the velocity field is weakest. Assuming that $\theta_\infty(1) = 0$ it then follows that there is a point z_0 such that $z_1 < z_0 < 1$ and $\theta'_\infty(z_0) = 0$. In other words, the temperature at the edge of the vertical boundary layer attains a maximum value above the point at which the horizontal velocity at the edge of the vertical boundary layer vanishes. This implies that for $z_0 < z < 1$ there are two roots (3.12) with positive real part (since $\phi'_\infty < 0$ and $\theta'_\infty < 0$ there), and that for $0 < z < z_0$ there is only one root (3.12) with positive real part (since $\theta'_\infty > 0$ there). These ideas are consistent with numerical and asymptotic results for finite values of L reported by Daniels & Punpocha (2004, 2005).

4. Asymptotic solution for $z \to 1$ and $z \to 0$

4.1. $z \to 1$

At the upper end of the vertical boundary layer

$$\phi_\infty = a_\infty(1 - z) + \cdots, \quad \theta_\infty = b_\infty(1 - z) + \cdots \text{ as } z \to 1, \tag{4.1}$$

where the coefficients a_∞ and b_∞ are determined by the solution in the core region. Within the vertical boundary layer

$$\phi = (1 - z)b_\infty^{1/2}\hat{f}(\hat{\xi}) + \cdots, \quad \theta = (1 - z)b_\infty(1 - \hat{f}') + \cdots \text{ as } z \to 1, \tag{4.2}$$

where $\xi = b_\infty^{-1/2}\hat{\xi}$ and $\hat{f}$ is the solution of a third-order ordinary differential equation given by Daniels & Punpocha (2005, equation (4.10)). This satisfies $\hat{f}(0) = \hat{f}''(0) = 0$ and has the behaviour $\hat{f} \to \hat{a}$ as $\hat{\xi} \to \infty$ where $\hat{a}$ varies from 0 to ∞ as $\hat{k} = \hat{f}'(0)$ varies from 0 to 1. The outer behaviour (4.1) requires that

$$\hat{a} = a_\infty b_\infty^{-1/2} \tag{4.3}$$

which in turn determines the value of $\hat{k}$ for any positive values of a_∞ and b_∞. Thus both ϕ_∞ and θ_∞ can be specified at the outer edge of the vertical boundary layer near $z = 1$, in agreement with the fact that both of the roots (3.12) have positive real part. The boundary-layer decay is oscillatory if $a_\infty b_\infty^{-1/2} < 2$, that is if the (adverse) vertical

https://doi.org/10.1017/S0022112006001868 Published online by Cambridge University Press

stratification is too great or the horizontal entrainment into the layer is too weak. The wall temperature is given by

$$\theta = (1-z)b_\infty(1-\hat{k}) + \cdots \text{ as } z \to 1 \tag{4.4}$$

and since $0 < \hat{k} < 1$ increases as z decreases from 1 but at a slower rate than the external temperature θ_∞.

4.2. $z \to 0$

At the lower end of the vertical boundary layer a solution consistent with the boundary conditions (3.4) applied in the core can be found with

$$\phi_\infty = az + \cdots, \quad \theta_\infty = b + cz^2 + \cdots, \tag{4.5}$$

where a, b and c are constants. Within the vertical boundary layer

$$\phi = zF(\eta) + \cdots, \quad \theta = b + z^2 G(\eta) + \cdots \text{ as } z \to 0, \tag{4.6}$$

where $\eta = \xi z$ and, from (3.7), the functions F and G satisfy the equations

$$F'' = -G', \quad G'F - 2GF' = 0. \tag{4.7}$$

This represents a convectively dominated flow in which $G = kF^2$ where k is a positive constant. A solution consistent with (4.5) requires that $F \to a, G \to c$ as $\eta \to \infty$ in which case $c = ka^2$ and F satisfies the equation $F' = k(a^2 - F^2)$. This has a solution satisfying the wall condition $F(0) = 0$ given by

$$F = a\tanh(ak\eta) \tag{4.8}$$

and then

$$G = a^2 k \tanh^2(ak\eta). \tag{4.9}$$

The constant k is not determined by this local analysis and its value is effectively fixed by the upstream history of the boundary layer, as is the value of the constant b in (4.5). Thus if ϕ_∞, through the value of a, is viewed as specified by the core solution, then the vertical boundary layer determines the corresponding form of θ_∞ near $z = 0$. This is consistent with the fact that if $a > 0$ and $c > 0$ so that locally $\phi'_\infty > 0$ and $\theta'_\infty > 0$, only one of the roots (3.12) has positive real part.

The effects of thermal conduction are too small to influence equations (4.7), indicating the possible existence of an inner thermal layer where $\xi \sim z^{-1/2}$ as $z \to 0$. Within this layer

$$\phi = z^{3/2}\tilde{F}(\gamma) + \cdots, \quad \theta = b + z^3\tilde{G}(\gamma) \text{ as } z \to 0, \tag{4.10}$$

where $\gamma = \xi z^{1/2}$. Since $\tilde{F}'' = 0$ it follows from matching with (4.6) that $\tilde{F} = a^2 k\gamma$ and then $\tilde{G}$ is found to satisfy the equation

$$\tilde{G}'' - \tfrac{3}{2}a^2 k\gamma\tilde{G}' + 3a^2 k\tilde{G} = 0, \tag{4.11}$$

with boundary conditions

$$\tilde{G}' = 0 \text{ at } \gamma = 0, \quad \tilde{G} \sim a^4 k^3 \gamma^2 \text{ as } \gamma \to \infty. \tag{4.12}$$

The required solution is

$$\tilde{G} = a^2 k^2 \left(a^2 k\gamma^2 - \tfrac{2}{3}\right). \tag{4.13}$$

Its relatively simple form is a consequence of the fact that the functional relation between temperature and stream function in the outer region where $\xi \sim z^{-1}$ results in a solution (4.9) already consistent with the thermal boundary condition at the sidewall. Indeed, the fact that the temperature is proportional to the square of the

https://doi.org/10.1017/S0022112006001868 Published online by Cambridge University Press

stream function in the outer region is essential as it ensures that the exponentially large complementary solution of the inner equation is not generated.

Note from (4.9) that the wall temperature is given by

$$\theta \sim b - \tfrac{2}{3}a^2k^2z^3 \text{ as } z \to 0, \tag{4.14}$$

suggesting that it increases monotonically from zero at the upper corner to the value b at the lower corner.

The width of the vertical boundary layer increases in a singular fashion as $z \to 0$, with $\xi \sim z^{-1/2}$ in the inner thermal layer and $\xi \sim z^{-1}$ in the outer layer. Sufficiently close to the lower wall the z-derivatives in the full governing equations (2.2) become comparable in size to the x-derivatives and the vertical boundary layer approximation breaks down. For the outer part of the layer this occurs when $x \sim z \sim R^{-1/4}$, leading to an outer corner zone where

$$\psi = R^{1/4}\Psi(\bar{x}, \bar{z}) + \cdots, \quad T = b + R^{-1/2}\Theta(\bar{x}, \bar{z}) + \cdots \tag{4.15}$$

and $x = R^{-1/4}\bar{x}$, $z = R^{-1/4}\bar{z}$. The governing equations are

$$\bar{\nabla}^2\Psi = -\frac{\partial\Theta}{\partial\bar{x}}, \quad \frac{\partial(\Theta, \Psi)}{\partial(\bar{x}, \bar{z})} = 0, \tag{4.16}$$

where $\bar{\nabla}^2 = \partial^2/\partial\bar{x}^2 + \partial^2/\partial\bar{z}^2$, from which it follows that $\Theta = k\Psi^2$ and Ψ satisfies the system

$$\bar{\nabla}^2\Psi + 2k\Psi\frac{\partial\Psi}{\partial\bar{x}} = 0, \tag{4.17}$$

$$\Psi = 0 \text{ on } \bar{x} = 0 \text{ and } \bar{z} = 0, \tag{4.18}$$

$$\Psi \sim \bar{z}F(\bar{x}\bar{z}) \text{ as } \bar{z} \to \infty, \tag{4.19}$$

$$\Psi \to a\bar{z} \text{ as } \bar{x} \to \infty, \tag{4.20}$$

where F is given by (4.8). Since conduction is neglected in (4.16), this corner zone also has conductive sublayers of thickness $x \sim R^{-3/8}$ and $z \sim R^{-3/8}$ on the sidewall and bottom wall respectively, within which $\psi \sim R^{1/8}$ and $T - b \sim R^{-3/4}$. Finally, an inner conductive corner zone occurs at the junction of the sublayers where $x \sim z \sim R^{-3/8}$, $\psi \sim 1$ and $T - b \sim R^{-1}$. Since all of these regions are passive and do not influence the overall flow or temperature fields in the cavity, or the leading-order value of the temperature in the corner, they will not be considered further here.

5. Numerical scheme

The numerical scheme used to solve the combined system (3.2)–(3.5) and (3.7)–(3.11) was based on that developed by Daniels & Punpocha (2005) for the finite-aspect-ratio cavity, modified to allow for the new behaviour near $z = 0$. Because the core region contains a two-way flow, steady-state solutions were found there using the artificial time-dependent system

$$\frac{\partial\bar{\phi}}{\partial t} = \frac{\partial^2\bar{\phi}}{\partial z^2} + \frac{\partial\bar{\theta}}{\partial X}, \quad \frac{\partial\bar{\theta}}{\partial t} = \frac{\partial^2\bar{\theta}}{\partial z^2} + \frac{\partial\bar{\phi}}{\partial X}\frac{\partial\bar{\theta}}{\partial z} - \frac{\partial\bar{\phi}}{\partial z}\frac{\partial\bar{\theta}}{\partial X}, \tag{5.1}$$

together with the boundary conditions (3.3)–(3.5) and the condition

$$\bar{\theta} = \theta_\infty(z) \text{ on } X = 0 \text{ for } z < z_0. \tag{5.2}$$

The system was discretized on a uniform mesh in X and z using central differences in X and z and a forward difference in time. Starting from a specified initial state

https://doi.org/10.1017/S0022112006001868 Published online by Cambridge University Press

this allows values of $\bar{\phi}$ and $\bar{\theta}$ to be determined explicitly for each new time step at all internal grid points. New values of $\bar{\theta}$ on $X=\bar{L}$ and $z=0$ are obtained using a quadratic extrapolation based on two internal grid points. No conditions are applied on $\bar{\theta}$ and $\bar{\phi}$ for $z \geqslant z_0$ at $X=0$ and new values are set there by using a quadratic extrapolation of the solution at three internal grid points. The same method is used to set the new values of $\bar{\phi}$ at $X=0$ in $z<z_0$; the values of $\bar{\theta}$ are fixed there by (5.2).

The next stage of the numerical scheme is to take the new steady-state profiles ϕ_∞ and θ_∞ (the latter for $z \geqslant z_0$ only) and use these as boundary conditions for ϕ and θ at the edge of the vertical boundary layer. The steady-state vertical boundary-layer equations are predominantly parabolic in the negative z-direction although small upward velocities occur near the edge of the layer if the outward exponential decay is oscillatory, which from (3.12) is the case in $z>z_0$ if $-\phi_\infty'(-\theta_\infty')^{-1/2}<2$. The solution was marched down the layer from the initial profile (3.8) at $z=1$. In order to capture the widening of the layer as $z\to 0$ a coordinate transformation $(\xi, z)\to(s, z)$ where $s=\xi\delta(z)$ was used, enabling the solution to be computed on a uniform grid in s and z over the domain $0\leqslant s\leqslant s_\infty, 0\leqslant z\leqslant 1$. The function $\delta(z)$ is chosen to be unity at $z=1$ and to have the asymptotic behaviour $\delta\sim\delta_0 z$ as $z\to 0$ to accommodate the asymptotic behaviour (4.6). The governing equations become

$$\delta\frac{\partial^2\phi}{\partial s^2}+\frac{\partial\theta}{\partial s}=0, \quad \delta\frac{\partial^2\theta}{\partial s^2}-\frac{\partial\phi}{\partial z}\frac{\partial\theta}{\partial s}+\frac{\partial\phi}{\partial s}\frac{\partial\theta}{\partial z}=0, \tag{5.3}$$

where ϕ and θ are now regarded as functions of s and z. These are solved subject to $\phi=\theta=0$ on $z=1$ and $\phi=\partial\theta/\partial s=0$ on $s=0$, together with $\phi\to\phi_\infty, \theta\to\theta_\infty$ as $s\to\infty$ for $z\geqslant z_0$ and $\phi\to\phi_\infty, \partial\phi/\partial s\to 0$ as $s\to\infty$ for $z<z_0$. The equations were converted to first-order form and the Crank–Nicolson method together with Newton iteration used to solve them, applying the edge conditions at $s=s_\infty$.

The overall scheme consisted of successive computations of the core region and vertical boundary layer until convergence was achieved. The computation can lead to a change in z_0 depending on the behaviour of $\bar{\theta}$ at $X=0$. In practice an adjustment to z_0 was made before each solution of the core region to ensure that $\partial\bar{\theta}(0, z)/\partial z$ remained zero at $z=z_0+$. Such adjustments were limited to a change of at most one step length in the z-direction at any given stage.

For a given value of $\bar{L}$, the entire scheme was started using

$$\bar{\phi}=\left(1-\frac{X}{\bar{L}}\right)\phi_\infty(z), \quad \bar{\theta}=\theta_\infty(z)+\left(1-\left(1-\frac{X}{\bar{L}}\right)^2\right)\left(1-\alpha_0\cos\frac{\pi z}{2}\right) \tag{5.4}$$

as the initial state at $t=0$ in the core region, with

$$\phi_\infty=4z(1-z)\phi_{\infty\max}, \tag{5.5}$$

$$\theta_\infty=\theta_{\infty\max}\left(\frac{1-z}{1-z_0}\right)\left(2-\frac{1-z}{1-z_0}\right), \quad z>z_0, \tag{5.6}$$

$$\theta_\infty=\frac{1}{2}\left(\theta_0+\theta_{\infty\max}+(\theta_0-\theta_{\infty\max})\cos\frac{\pi z}{z_0}\right), \quad z<z_0 \tag{5.7}$$

and values of $z_0, \phi_{\infty\max}, \theta_{\infty\max}, \theta_0$ and α_0 chosen by reference to computations for previous values of $\bar{L}$ or, in the first instance, the solution computed by Daniels & Punpocha (2005), which is equivalent to the limiting case $\bar{L}\to 0$ (see § 7 below). The initial state (5.4) was also used for subsequent computations of the core region but with ϕ_∞ and θ_∞ replaced by their latest approximations.

https://doi.org/10.1017/S0022112006001868 Published online by Cambridge University Press

6. Results

Various checks were made to test the dependence of the numerical solution on the various step sizes involved and on the implementation of the boundary conditions and initial conditions. One possible source of error is a limitation on s_∞ to avoid numerical instability at the outer edge of the vertical boundary layer in $z > z_0$, but this is only of any significance near $z = 1$ where the value of $-\phi'_\infty(-\theta'_\infty)^{-1/2}$ is minimum. In the final converged state the results to be presented below indicate that the value of $\hat{a}$ in (4.3) ranges typically from 1.4 when $\bar{L} = 0.05$ to 1.6 when $\bar{L} = 1$. Although oscillatory behaviour occurs strictly when $\hat{a} < 2$, it remains small if $\hat{a} > 1.4$ (see Daniels & Punpocha 2005, section 7) and since the value of $-\phi'_\infty(-\theta'_\infty)^{-1/2}$ quickly rises above the value 2 as z decreases from 1, any impact on the solution is small. The most accurate computations were performed with 100 steps in the z-direction, 40 steps in X and 60 steps in s and in this case the errors in the temperature and stream function are estimated to be less than 0.5 %.

In the vertical layer it was found necessary to choose the transformation function $\delta(z)$ carefully both to avoid any instability associated with reverse flow at the edge of the layer and to ensure a sufficiently large outer boundary for all values of z. For moderate values of $\bar{L}$ (in the range $0.1 < \bar{L} < 0.6$) the form

$$\delta(z) = 1 + \alpha(z-1) \text{ for } z \geqslant z_a, \tag{6.1}$$

$$\delta(z) = 1 + \alpha(z-1) + (\alpha - 1)\exp\left(\frac{z}{z_a(z-z_a)}\right) \text{ for } z < z_a \tag{6.2}$$

was used, with the value of z_a usually chosen to coincide with the initial estimate for z_0. It was found convenient to recompute the solution in the region $z \geqslant z_0$ and adjust the parameter α until the value of $\partial\phi/\partial s$ at $s = s_\infty$ was zero (to at least six decimal places) at $z = z_0+$. Since $\delta\partial\phi/\partial s = \theta_\infty - \theta$ and the left-hand side is zero at $s = s_\infty$ for $z < z_0$, this ensures a smooth transition in the value of θ_∞ across $z = z_0$. The remainder of the vertical boundary layer is then computed from $z = z_0$ to $z = 0$. Typical initial values used for α ranged from 2 for $\bar{L} = 0.1$ to 1.6 for $\bar{L} = 0.6$.

For extreme values of $\bar{L}$ ($\bar{L} = 0.025, 0.05, 0.8$ and 1) it was found necessary to replace (6.2) by a two-part definition of δ such that, in the region $z \leqslant z_b$, δ is defined by the linear form $\delta(z) = \beta z$ and, in the region $z_b < z < z_a$, by a quartic polynomial in z with continuous function values and first derivatives at $z = z_a$ and $z = z_b$. The parameters z_a, z_b, α and β are all suitably chosen and α is again used as an adjustable parameter to recompute the solution in $z > z_0$.

The vertical boundary layer widens as $\bar{L}$ increases, so that it was also necessary to adjust s_∞ accordingly, with typical values ranging from 0.195 for $\bar{L} = 0.025$ to 10.8 for $\bar{L} = 1$.

In the core region, stability limitations of the explicit scheme necessitated the use of a small time step $\Delta t = 10^{-5}$ and 2×10^5 time steps were generally sufficient to achieve convergence such that the numerical approximations to $\bar{\phi}$ and $\bar{\theta}$ were steady to at least six significant figures.

Provided the choice of the various parameters involved in the initial state and the transformation function $\delta(z)$ were reasonable, the entire scheme generally converged to the final solution within about 20 overall iterations of the core/vertical boundary-layer systems. Figure 2 shows a summary of the main properties of the solution as a function of $\bar{L}$. The temperature is shown at the corners and the midpoint of the lower boundary. Also shown are the maximum values of the temperature and stream function at the edge of the vertical boundary layer, together with the heights $z = z_0$

https://doi.org/10.1017/S0022112006001868 Published online by Cambridge University Press

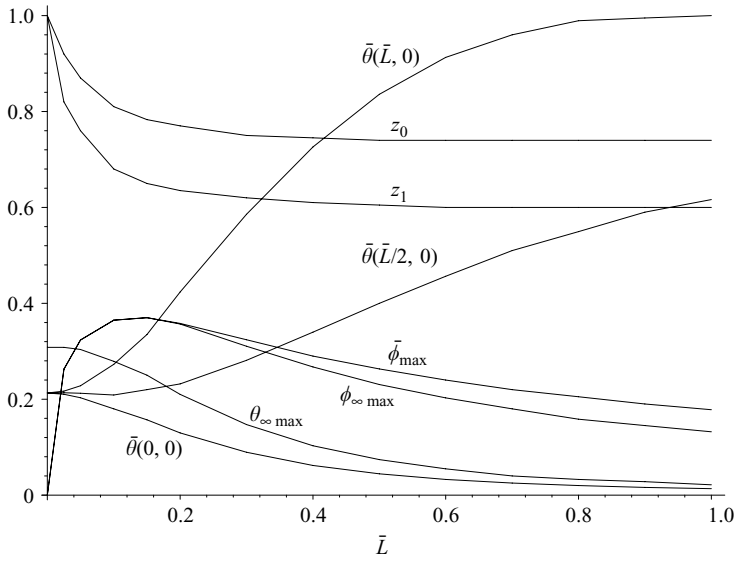


FIGURE 2. Main solution properties as a function of $\bar{L}$ showing the core temperatures $\bar{\theta}(0, 0)$, $\bar{\theta}(\bar{L}/2, 0)$, $\bar{\theta}(\bar{L}, 0)$, the maximum values of the temperature and stream function at the edge of the vertical boundary layer, $\theta_{\infty\,\max}$, $\phi_{\infty\,\max}$, and their respective locations z_0, z_1, and the overall maximum value of the stream function $\bar{\phi}_{\max}$.

and $z = z_1$ at which they occur. The overall stream function maximum is also shown. As $\bar{L}$ increases, the centre of circulation moves away from the edge of the vertical boundary layer into the end of the core region and the width of the vertical boundary layer increases. The overall stream function maximum reaches a maximum value as a function of $\bar{L}$ at $\bar{L} = 0.13$.

Figures 3 to 11 show details of the solution for $\bar{L} = 0.05, 0.2$ and 1, corresponding to low, moderate and high values of the parameter $\bar{L}$. The profiles ϕ_∞ and θ_∞ at the edge of the vertical boundary layer are shown in figure 3. For $\bar{L} = 0.05$ the centre of circulation occurs at the edge of the vertical boundary layer near the top of the cold wall and locally there is a strong flow along the upper wall and down the vertical boundary layer. In the core, the isotherms and streamlines shown in figure 4 are tightly packed near the upper surface of the cavity, where the major variation in the horizontal flow and temperature occurs; this variation is shown in figure 5. As $\bar{L}$ increases, the centre of circulation moves downwards and into the core region, as shown by the core isotherms and streamlines for $\bar{L} = 0.2$ in figure 6. The isotherms now tilt downwards relative to the cavity walls as conduction becomes more significant throughout the flow and the return flow in the lower half of the cavity strengthens, as shown in figure 7. Profiles of the vertical velocity and temperature in the vertical boundary layer shown in figure 8 indicate the manner in which the layer widens as $z \to 0$, consistent with the asymptotic behaviour predicted in § 4.2. For $\bar{L} = 1$ the core isotherms shown in figure 9 are almost vertical, an indication that conduction is now dominant throughout most of the cavity; the centre of circulation moves to a position at roughly mid-height and there is an almost symmetrical horizontal flow, as shown in figure 10. Finally, figure 11 shows that there is a significant overall widening of the vertical boundary layer and a reduction in the vertical flow speed there compared with the corresponding results for $\bar{L} = 0.2$ in figure 8. This is associated with the decrease in speed of the recirculating flow (as evidenced by the horizontal flow speeds

https://doi.org/10.1017/S0022112006001868 Published online by Cambridge University Press

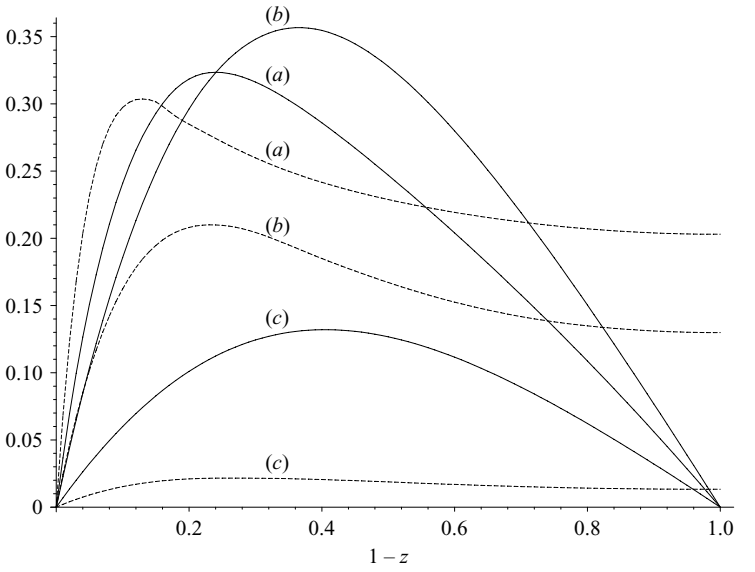


FIGURE 3. The profiles ϕ_∞ (—) and θ_∞ (- - -) at the edge of the vertical boundary layer for (*a*) $\bar{L} = 0.05$, (*b*) $\bar{L} = 0.2$, (*c*) $\bar{L} = 1$.

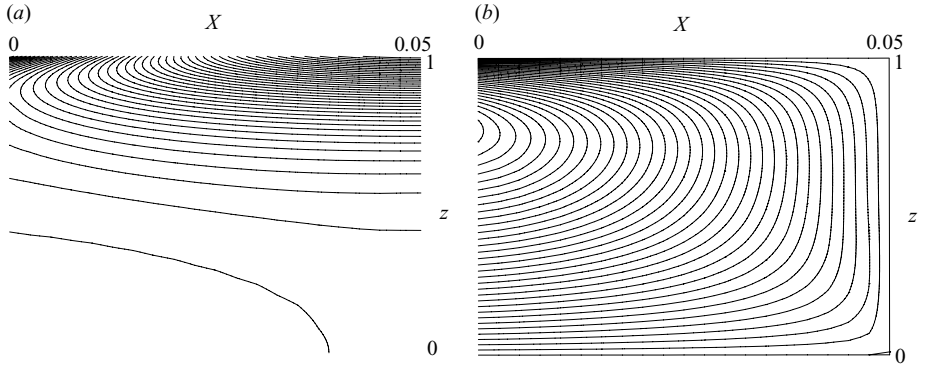


FIGURE 4. (*a*) Isotherms and (*b*) streamlines of the core solution for $\bar{L} = 0.05$. The flow is counterclockwise and the intervals in $\bar{\theta}$ and $\bar{\phi}$ are 0.02 and 0.01 respectively.

in figures 7 and 10) and with the reduction in thermal gradients near the cold sidewall as $\bar{L}$ increases.

7. Discussion

Solutions have been found for the flow and temperature fields within a cavity differentially heated at the upper surface for large aspect ratios L and high Darcy–Rayleigh numbers R such that $\bar{L} = LR^{-1/2}$ is of order one. A single-cell circulation is generated in which fluid circulates between the main core region and a vertical boundary layer of width order $R^{-1/2}$ near the colder sidewall. For fixed R, equivalent to a fixed temperature differential ΔT and cavity height h, variations in $\bar{L}$ are equivalent to variations in the length d of the cavity. For the quadratic profile (2.8),

https://doi.org/10.1017/S0022112006001868 Published online by Cambridge University Press

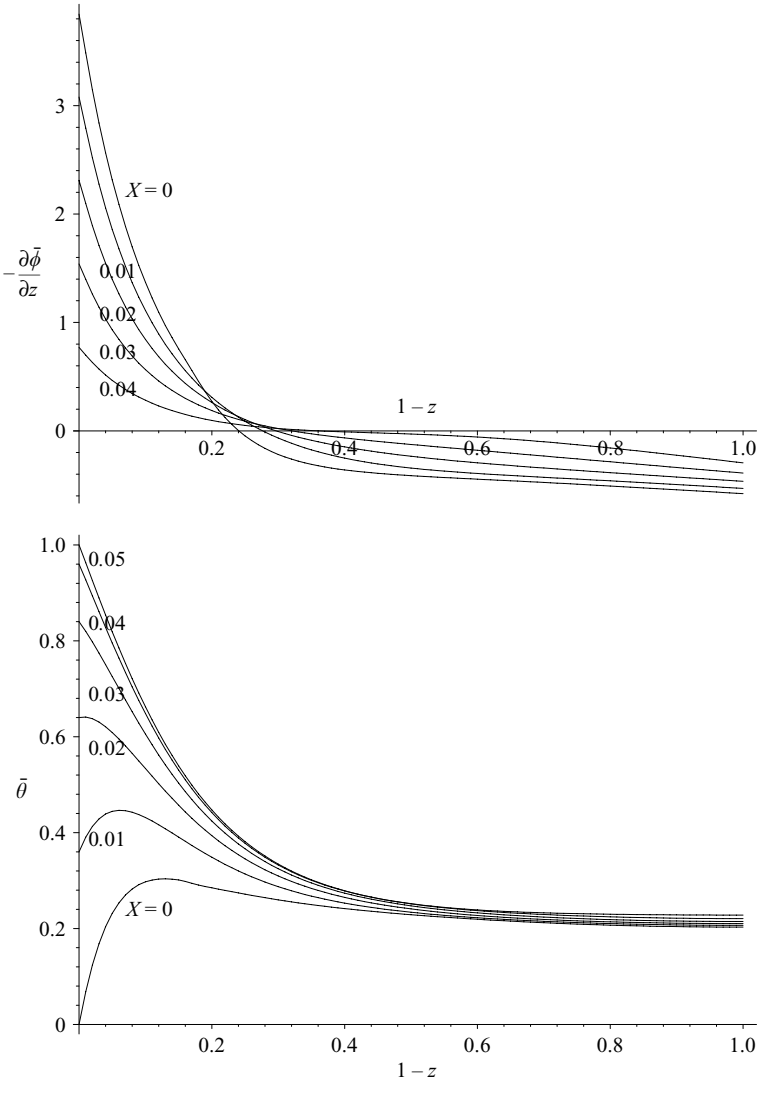


FIGURE 5. Horizontal velocity and temperature profiles in the core region for $\bar{L}=0.05$.

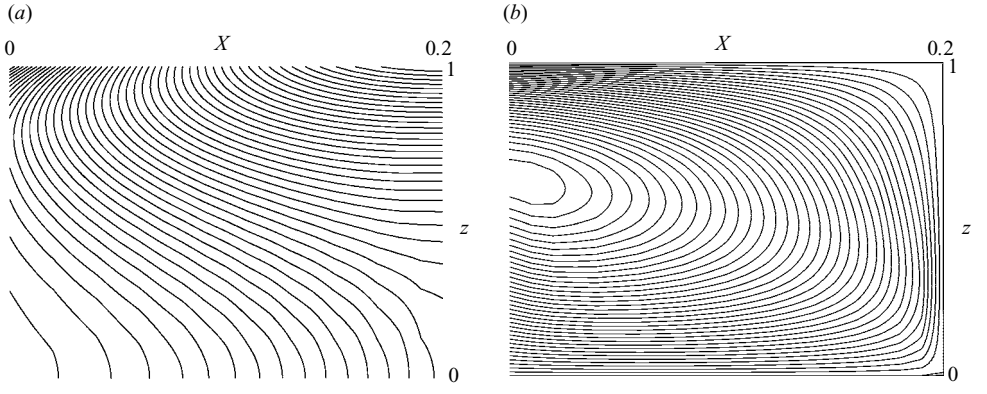


FIGURE 6. (*a*) Isotherms and (*b*) streamlines of the core solution for $\bar{L}=0.2$. The flow is counterclockwise and the intervals in $\bar{\theta}$ and $\bar{\phi}$ are 0.02 and 0.01 respectively.

https://doi.org/10.1017/S0022112006001868 Published online by Cambridge University Press

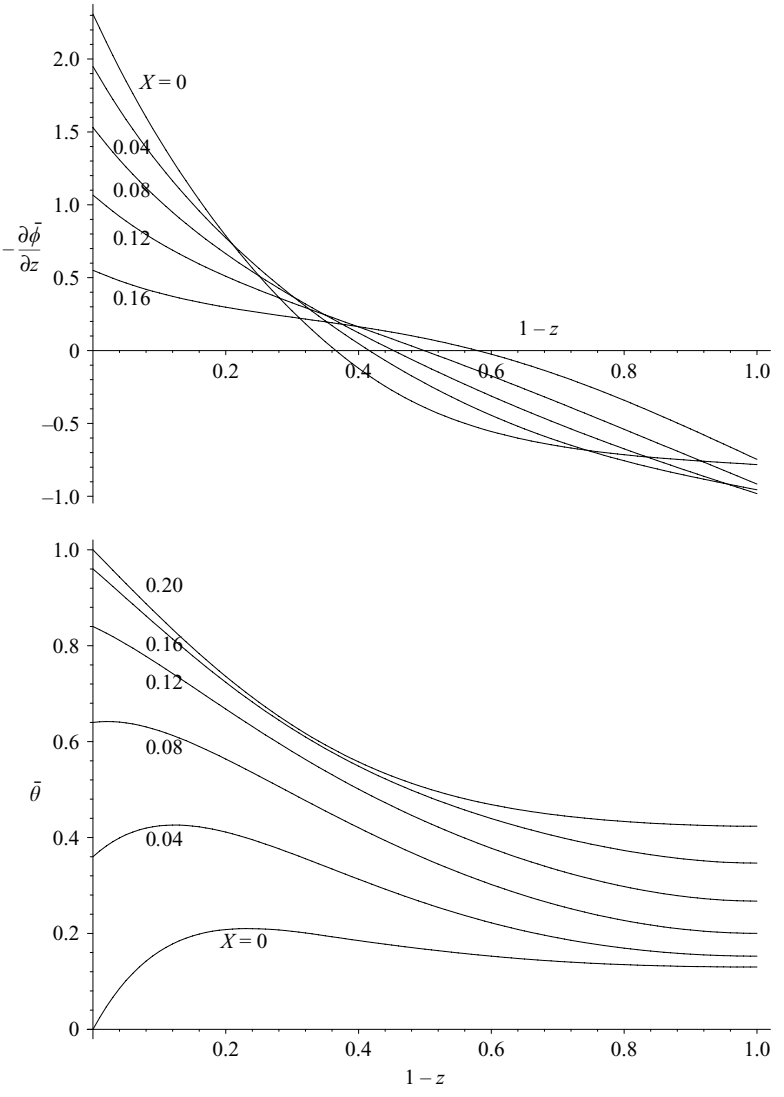


FIGURE 7. Horizontal velocity and temperature profiles in the core region for $\bar{L} = 0.2$.

the present results show that as $\bar{L}$ increases the circulation driven by the temperature differential reaches maximum intensity at $\bar{L} = 0.13$ and then subsides. This critical value of $\bar{L}$ can be expected to depend on the precise form of the temperature profile S at the upper surface, although general features of the flow, such as the asymptotic properties described in § 4, are applicable for any monotonic form of S.

At low values of $\bar{L}$, the circulation occurs primarily near the upper surface within a horizontal boundary layer of depth order $1 - z \sim \bar{L}^{2/3}$ and the vertical boundary layer of width $\xi \sim \bar{L}^{1/3}$. The structure of the solution in this limit is that of high Darcy–Rayleigh number flow in a cavity of finite aspect ratio (Daniels & Punpocha 2005). For the quadratic profile (2.8), the temperature and stream function attain maximum values

$$T \sim 0.308, \quad \psi \sim 0.889 R^{1/2} \bar{L}^{1/3} \tag{7.1}$$

https://doi.org/10.1017/S0022112006001868 Published online by Cambridge University Press

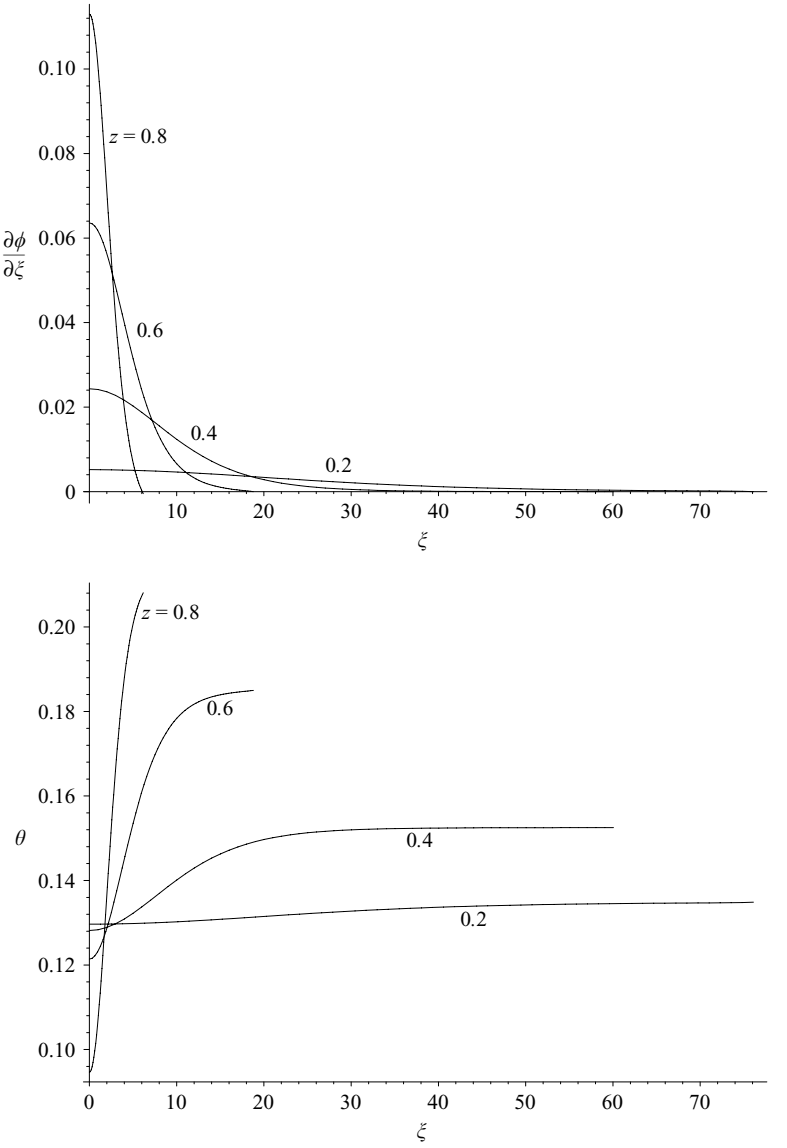


FIGURE 8. Vertical velocity and temperature profiles in the vertical boundary layer for $\bar{L} = 0.2$.

at the edge of the vertical boundary layer, at depths

$$1 - z_0 \sim 1.00\bar{L}^{2/3}, \quad 1 - z_1 \sim 2.10\bar{L}^{2/3} \tag{7.2}$$

respectively. Below the upper surface layer, the cavity is at near-constant temperature

$$T \sim 0.213 + O(\bar{L}^2), \quad \bar{L} \to 0. \tag{7.3}$$

The asymptotic results (7.1)–(7.3) are in good agreement with the numerical results of § 6. As $\bar{L} \to 0$ the present theory encompasses the horizontal/vertical boundary-layer structure of Daniels & Punpocha (2005) and so correctly predicts the position of the centre of circulation even when $L = O(1)$. It does not, however, encompass the leading-order variations of the flow and temperature within the core region when

https://doi.org/10.1017/S0022112006001868 Published online by Cambridge University Press

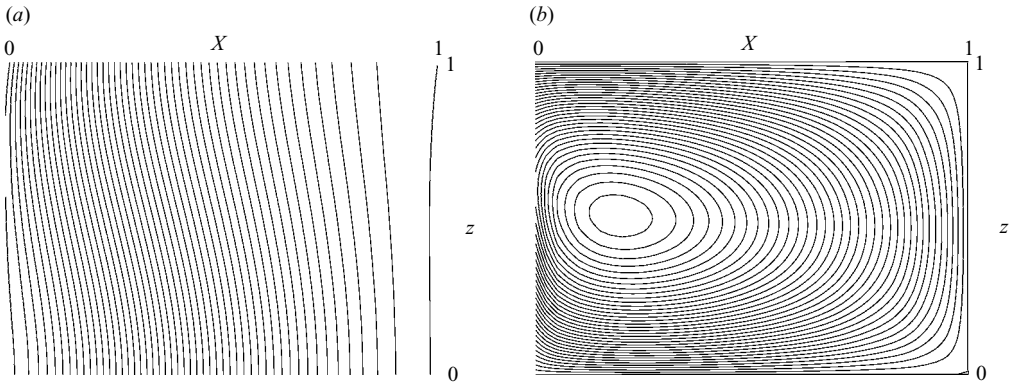


FIGURE 9. (*a*) Isotherms and (*b*) streamlines of the core solution for $\bar{L} = 1$. The flow is counterclockwise and the intervals in $\bar{\theta}$ and $\bar{\phi}$ are 0.02 and 0.005 respectively.

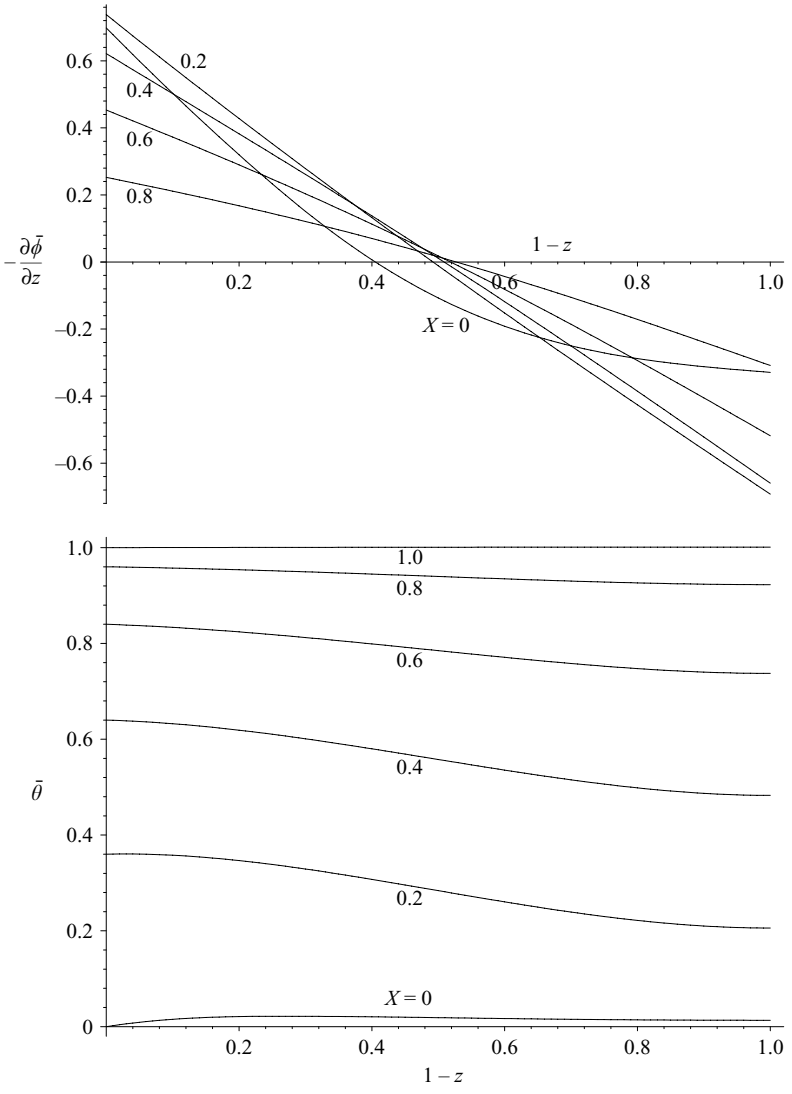


FIGURE 10. Horizontal velocity and temperature profiles in the core region for $\bar{L} = 1$.

https://doi.org/10.1017/S0022112006001868 Published online by Cambridge University Press

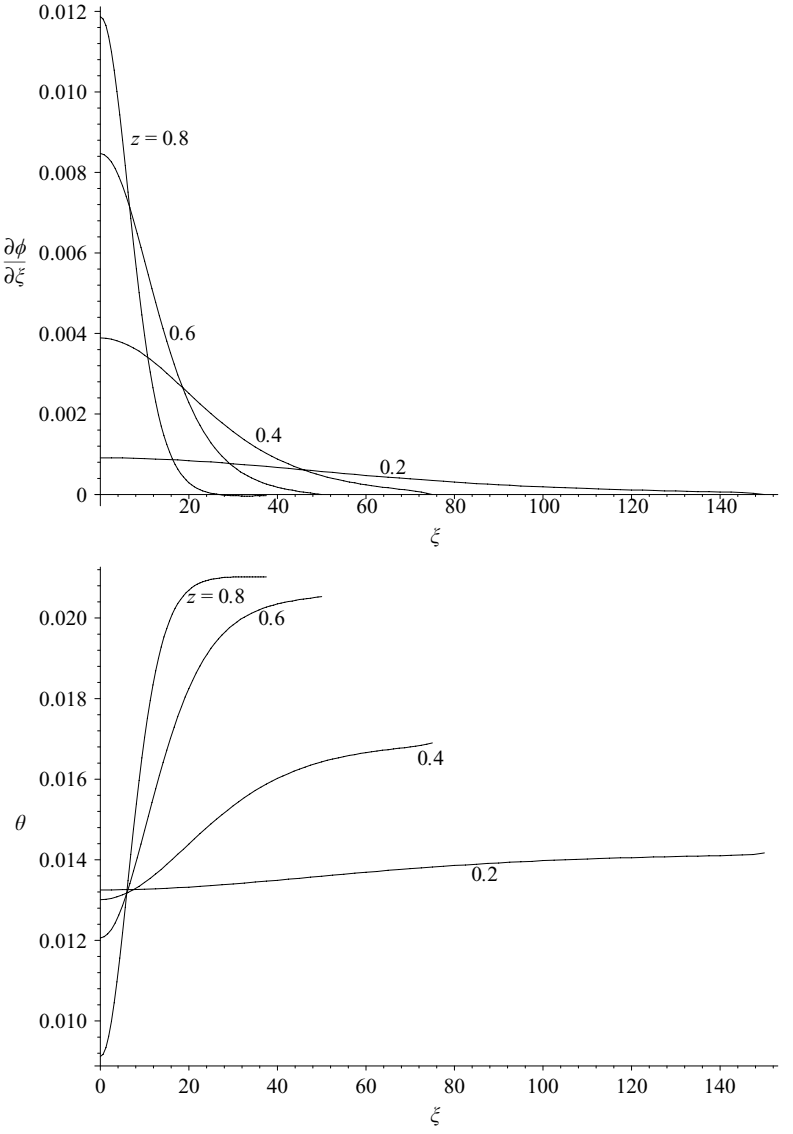


FIGURE 11. Vertical velocity and temperature profiles in the vertical boundary layer for $\bar{L} = 1$.

$L = O(1)$ because these are governed by the full equations of motion. For even smaller aspect ratios $L = O(R^{-1})$ the vertical and horizontal boundary layers merge to form a single zone near the upper surface of the cavity where $x \sim 1 - z \sim L \sim R^{-1}$. The centre of circulation within this region is then determined by the full equations of motion and the present theory is no longer applicable.

The lower boundary of the cavity has a significant impact on the flow at finite values of $\bar{L}$, and as $\bar{L} \to \infty$ the core region becomes dominated by conduction. For the quadratic profile (2.8), as $\bar{L} \to \infty$ the solutions of (3.2) for the temperature and stream function that satisfy the boundary conditions at $z = 0$ and $z = 1$ are

$$\bar{\theta} = 1 - (1 - \bar{X})^2 + \bar{L}^{-2}(1 - \bar{X})^2\left(z^2 - \tfrac{2}{3}z^3 - \tfrac{1}{3}\right) + \cdots, \tag{7.4}$$

$$\bar{\phi} = \bar{L}^{-1}(1 - \bar{X})z(1 - z) + \cdots, \tag{7.5}$$

https://doi.org/10.1017/S0022112006001868 Published online by Cambridge University Press

where $\bar{X} = X/\bar{L}$. These solutions also satisfy the boundary conditions at the hotter end of the cavity, $\bar{X} = 1$. At the colder end, $\bar{X} = 0$, the solution (7.4), (7.5) does not match directly with the vertical boundary layer. Instead there is an inner core region where $\hat{X} = X\bar{L}$ is of order one and

$$\bar{\theta} = \bar{L}^{-2}\hat{\theta}(\hat{X}, z) + \cdots, \quad \bar{\phi} = \bar{L}^{-1}\hat{\phi}(\hat{X}, z) + \cdots. \tag{7.6}$$

This is governed by the horizontal boundary-layer equations

$$\frac{\partial^2\hat{\phi}}{\partial z^2} = -\frac{\partial\hat{\theta}}{\partial\hat{X}}, \quad \frac{\partial^2\hat{\theta}}{\partial z^2} = \frac{\partial\hat{\phi}}{\partial z}\frac{\partial\hat{\theta}}{\partial\hat{X}} - \frac{\partial\hat{\phi}}{\partial\hat{X}}\frac{\partial\hat{\theta}}{\partial z}. \tag{7.7}$$

The functions $\hat{\theta}$ and $\hat{\phi}$ satisfy the boundary conditions

$$\hat{\theta} = 2\hat{X}, \quad \hat{\phi} = 0 \text{ at } z = 1, \tag{7.8}$$

$$\frac{\partial\hat{\theta}}{\partial z} = \hat{\phi} = 0 \text{ at } z = 0, \tag{7.9}$$

and matching with (7.4) and (7.5) requires that

$$\hat{\theta} \sim 2\hat{X} + \left(z^2 - \tfrac{2}{3}z^3 - \tfrac{1}{3}\right), \quad \hat{\phi} \to z(1-z) \text{ as } \hat{X} \to \infty. \tag{7.10}$$

Within the vertical boundary layer,

$$\theta = \bar{L}^{-2}\tilde{\theta}(\tilde{\xi}, z) + \cdots, \quad \phi = \bar{L}^{-1}\tilde{\phi}(\tilde{\xi}, z) + \cdots \text{ as } \bar{L} \to \infty, \tag{7.11}$$

where $\xi = \bar{L}\tilde{\xi}$ and the functions $\tilde{\theta}$ and $\tilde{\phi}$ satisfy the equations

$$\frac{\partial^2\tilde{\phi}}{\partial\tilde{\xi}^2} = -\frac{\partial\tilde{\theta}}{\partial\tilde{\xi}}, \quad \frac{\partial^2\tilde{\theta}}{\partial\tilde{\xi}^2} = \frac{\partial\tilde{\phi}}{\partial z}\frac{\partial\tilde{\theta}}{\partial\tilde{\xi}} - \frac{\partial\tilde{\phi}}{\partial\tilde{\xi}}\frac{\partial\tilde{\theta}}{\partial z} \tag{7.12}$$

and boundary conditions

$$\tilde{\phi} = 0, \quad \tilde{\theta} = 0 \text{ on } z = 1, \tag{7.13}$$

$$\tilde{\phi} = \frac{\partial\tilde{\theta}}{\partial\tilde{\xi}} = 0 \text{ on } \tilde{\xi} = 0, \tag{7.14}$$

$$\tilde{\phi} \to \tilde{\phi}_\infty, \quad \tilde{\theta} \to \tilde{\theta}_\infty \text{ as } \tilde{\xi} \to \infty. \tag{7.15}$$

Finally, matching with the inner core region requires that

$$\tilde{\phi}_\infty = \hat{\phi}(0, z), \quad \tilde{\theta}_\infty = \hat{\theta}(0, z). \tag{7.16}$$

The combined systems (7.7)–(7.10) and (7.12)–(7.16) are similar to those of the full problem for finite $\bar{L}$ and would again require an interactive numerical solution. This is not undertaken here. However, it is noted that the inner core region effects the transition from the vertical boundary-layer profile $\tilde{\phi}_\infty$ at $\hat{X} = 0$ to the profile $z(1-z)$ as $\hat{X} \to \infty$, which corresponds to an antisymmetric two-way flow throughout the main part of the cavity. This is consistent with the flow pattern observed in figure 9 and with the existence of the centre of circulation within the inner core region. As far as the temperature field is concerned, the inner core region effects a transition from the profile $\tilde{\theta}_\infty$ at $\hat{X} = 0$, which has a maximum at $z_0 > z_1$, to the profile associated with (7.10) which is monotonic in z and has a maximum value at $z = 1$.

The scaling of ξ as $\bar{L} \to \infty$ confirms that the width of the vertical boundary layer increases with $\bar{L}$, consistent with the numerical results described in § 6. Eventually, the vertical boundary-layer width

$$x = R^{-1/2}\xi \sim R^{-1/2}\bar{L} \tag{7.17}$$

https://doi.org/10.1017/S0022112006001868 Published online by Cambridge University Press

becomes comparable with the width of the inner core region,

$$x = R^{1/2}X \sim R^{1/2}\bar{L}^{-1}, \tag{7.18}$$

when $\bar{L} \sim R^{1/2}$ and $x \sim 1$. In this new regime, where $L = O(R)$, the asymptotic structure of the solution consists of a core region in which (7.4), (7.5) apply and an end region $0 < x < \infty$, $0 < z < 1$ where $T \sim L^{-1}$ and $\psi \sim 1$. Nonlinear convective effects are confined to the end region which is governed by the full equations (2.2) for finite values of R/L. An analytical solution of the end-region problem can be obtained in the limit as $R/L \to 0$ and is given by

$$T \sim \frac{1}{L}\left\{2x + \frac{16}{\pi^2}\sum_{m=0}^{\infty}\frac{(-1)^m}{(2m+1)^2}\mathrm{e}^{-(2m+1)\pi x/2}\cos\frac{(2m+1)\pi z}{2}\right\}, \tag{7.19}$$

$$\begin{aligned}\psi \sim \frac{R}{L}\Bigg\{&z(1-z) + \sum_{m=0}^{\infty}\Bigg(\frac{256(-1)^m}{\pi^4(2m+1)}\sum_{n=1}^{\infty}\frac{n}{((2m+1)^2-4n^2)^2}\mathrm{e}^{-n\pi x}\sin n\pi z\\ &+\frac{8(-1)^m}{\pi^2(2m+1)^2}\mathrm{e}^{-(2m+1)\pi x/2}(z-1)\sin\frac{(2m+1)\pi z}{2}\\ &-\frac{8}{\pi^3(2m+1)^3}\mathrm{e}^{-(2m+1)\pi x}\sin(2m+1)\pi z\Bigg)\Bigg\}.\end{aligned} \tag{7.20}$$

In this limit the solution is conduction-dominated throughout the cavity.

Based on the preceding discussion, a quantitative estimate of the range of validity of the present theory can now be made. At small aspect ratios the key requirement is that the vertical boundary layer width is much less than the width of the cavity. Near the centre of circulation the width of the vertical boundary layer can be estimated from the results of Daniels & Punpocha (2005, figure 11) and written in the present notation as $\xi \sim 20\bar{L}^{1/3}$, so that the requirement that $x = R^{-1/2}\xi$ is much less than the cavity width gives $20R^{-1/2}\bar{L}^{1/3} \ll L$, or $20^{3/2}R^{-1} \ll L$. For large aspect ratios the present theory breaks down through the mechanism described by (7.17) and (7.18). Using the position of the centre of circulation in figure 9 ($X \sim 0.2\bar{L}^{-1}$) as a guide to the horizontal scale (7.18) and the vertical boundary-layer width at $z = 0.5$ from figure 11 ($\xi \sim 40\bar{L}$) as a guide to the horizontal scale (7.17), this suggests that validity of the present theory requires $40\bar{L}R^{-1/2} \ll 0.2\bar{L}^{-1}R^{1/2}$, or $L \ll 200^{-1/2}R$. Combining this with the earlier result for small $\bar{L}$ suggests that validity of the present large Darcy–Rayleigh number theory requires the cavity width to be in the range

$$20^{3/2}R^{-1} \ll L \ll 200^{-1/2}R. \tag{7.21}$$

This predicts an increasingly wide range of applicability of the theory as R increases. For $R = 1000$ the range is approximately $0.1 \ll L \ll 70$ and even at $R = 100$ there is a viable range $1 \ll L \ll 7$ within which the theory should provide a good approximation. This can be tested by comparing the results of the present theory with numerical calculations for the temperature profile (2.8) reported by Punpocha (2000). Table 1 shows the height z of the centre of circulation for a range of values of R and L. As expected, the prediction is poor at low values of R when $L = 1$ but for $L = 4$ is accurate to within an error of less than 1 % for all values of R in the range 30 to 5000.

The present theory for the flow driven from above by a buoyancy sink applies equally to flows driven from below by a buoyancy source (via the transformation

https://doi.org/10.1017/S0022112006001868 Published online by Cambridge University Press

	$L=1$			$L=2$			$L=4$		
R	$\bar{L}$	Theory	Numerical	$\bar{L}$	Theory	Numerical	$\bar{L}$	Theory	Numerical
30	0.183	0.64	0.70	0.365	0.55	0.57	0.730	0.52	0.52
200	0.071	0.73	0.76	0.141	0.64	0.65	0.283	0.58	0.58
500	0.045	0.78	0.81	0.089	0.70	0.71	0.179	0.63	0.63
1500	0.026	0.83	0.86	0.052	0.76	0.77	0.103	0.68	0.68
5000	0.014	0.89	0.90	0.028	0.82	0.83	0.057	0.75	0.75

TABLE 1. Vertical location z of the centre of circulation predicted by the present theory and by the numerical calculations of Punpocha (2000) for various values of R and L.

$T \to 1-T$, $\psi \to \psi$, $x \to L-x$, $z \to 1-z$), of interest in relation to motions generated within geothermal energy reservoirs. The sidewall conditions $\psi = \partial T/\partial x = 0$ assumed here are the same as those applicable to the plane of symmetry of a two-dimensional plume driven by symmetric heating from below, as discussed by Phillips (1991, section 7.6). In this plume problem the ambient temperature is generally viewed as specified at a level below that of the heat source and there is a net upward heat flux through the system, whereas in the problem studied here the net vertical heat flux is zero. However, near the sidewall where the vertical thermal gradient is negative, the flow studied here is equivalent to that of a plume.

REFERENCES

BLYTHE, P. A., SIMPKINS, P. G. & DANIELS, P. G. 1983 Thermal convection in a cavity filled with a porous medium: a classification of limiting behaviours. *Intl J. Heat Mass Transfer* **26**, 701–708.

DANIELS, P. G., BLYTHE, P. A. & SIMPKINS, P. G. 1986 Thermally driven shallow cavity flows in porous media: the intermediate regime. *Proc. R. Soc. Lond.* A **406**, 263–285.

DANIELS, P. G., BLYTHE, P. A. & SIMPKINS, P. G. 1989 Thermally driven cavity flows in porous media: the merged-layer regime. *Proc. R. Soc. Lond.* A **426**, 107–124.

DANIELS, P. G. & PUNPOCHA, M. 2004 Cavity flow in a porous medium driven by differential heating. *Intl J. Heat Mass Transfer* **47**, 3017–3030.

DANIELS, P. G. & PUNPOCHA, M. 2005 On the boundary-layer structure of cavity flow in a porous medium driven by differential heating. *J. Fluid Mech.* **532**, 321–344.

LAPWOOD, E. R. 1948 Convection of a fluid in a porous medium. *Proc. Camb. Phil. Soc.* **44**, 508–521.

PHILLIPS, O. M. 1991 *Flow and Reactions in Permeable Rocks*. Cambridge University Press.

PUNPOCHA, M. 2000 Flow in a porous medium driven by differential heating. PhD thesis. City University, London.

REES, D. A. S. 2000 The stability of Darcy-Benard convection. In *Handbook of Porous Media* (ed. K. Vafai), pp. 521–558. Marcel Dekker.

WALKER, K. L. & HOMSY, G. M. 1978 Convection in a porous cavity. *J. Fluid Mech.* **87**, 449–474.

https://doi.org/10.1017/S0022112006001868 Published online by Cambridge University Press